Laser-Induced Nanoscale Thermocapillary Flow for Purification of Aligned Arrays of Single-Walled Carbon Nanotubes

Frank Du,[†] Jonathan R. Felts,[‡] Xu Xie,[†] Jizhou Song,[§] Yuhang Li,[△] Matthew R. Rosenberger,[⊥] Ahmad E. Islam,[†] Sun Hun Jin,[#] Simon N. Dunham,[†] Chenxi Zhang,[¶] William L. Wilson,[†] Yonggang Huang,[‖] William P. King,[⊥] and John A. Rogers[*,†]

[†]Department of Materials Science and Engineering and Frederick Seitz Materials Research Laboratory, University of Illinois at Urbana—Champaign, Urbana, Illinois 61801, United States, [‡]Department of Mechanical Engineering, Texas A&M University, College Station, Texas 77843, United States, [§]Department of Engineering Mechanics and Soft Matter Research Center, Zhejiang University, Hangzhou, Zhejiang 310027, China, [△]Institute of Solid Mechanics, Beihang University, Beijing 100191, China, [‖]Departments of Civil and Environmental Engineering, Northwestern University, Evanston, Illinois 60208, United States, [⊥]Department of Mechanical Science and Engineering, University of Illinois at Urbana—Champaign, Urbana, Illinois 61801, United States, [#]Department of Electronic Engineering, Incheon National University, Incheon 406-772, Republic of Korea, and [¶]Department of Mechanical and Aerospace Engineering, University of Miami, Coral Gables, Florida 33157, United States

ABSTRACT Although aligned arrays of single-walled carbon nanotubes (SWNTs) have outstanding potential for use in broad classes of advanced semiconductor devices, the relatively large population of metallic SWNTs (m-SWNTs) that results from conventional growth techniques leads to significantly degraded performance. Recently reported methods based on thermocapillary effects that enable removal of m-SWNTs from such arrays offer exceptional levels of efficiency, but the procedures are cumbersome and require multiple processing steps. Here we present a simple, robust alternative that yields pristine arrays of purely semiconducting SWNTs (s-SWNTs) by use of irradiation with an infrared laser. Selective absorption by m-SWNTs coated with a thin organic film initiates nanoscale thermocapillary flows that lead to exposure only of the m-SWNTs. Reactive ion etching eliminates the m-SWNTs without damaging the s-SWNTs; removal of the film completes the purification. Systematic experimental studies and computational modeling of the thermal physics illuminates the essential aspects of this process. Demonstrations include use of arrays of s-SWNTs formed in this manner as semiconducting channel materials in statistically relevant numbers of transistors to achieve both high mobilities (>900 $cm^2\ V^{-1}\ s^{-1}$) and switching ratios (>10^4). Statistical analysis indicates that the arrays contain at least 99.8% s-SWNTs and likely significantly higher.

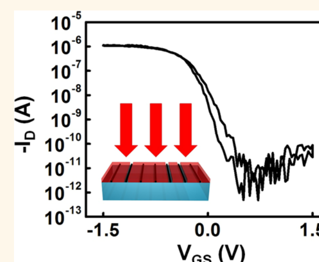

KEYWORDS: carbon · nanotube · SWNT · aligned array · purification · thin-film transistor · TFT · laser · infrared

Single-walled carbon nanotubes (SWNTs) remain of high interest to the electronic materials research community due to their unparalleled intrinsic electrical properties.[1,2] Semiconducting SWNTs exhibit carrier mobilities that can exceed 10^4 cm^2/Vs,[3] with ability to enable transistors with current switching ratios greater than 10^6.[2,4] Horizontally aligned arrays of SWNTs represent an ideal configuration for applications in electronics, where they serve as effective thin films that are process-compatible with conventional manufacturing strategies.[2,5] One means to produce such arrays involves chemical vapor deposition (CVD) on ST-cut quartz substrates to yield nearly perfectly straight SWNTs with nearly perfect alignment (>99.9% of SWNTs within 0.01° of the preferred growth direction).[6] In transistors, such arrays provide transport pathways from source to drain with effective performance that greatly exceeds that of randomly oriented networks of SWNTs due to the absence of tube-to-tube junctions.[7−9]

SWNT arrays grown using CVD techniques contain both metallic SWNTs (m-SWNTs) and semiconducting SWNTs

* Address correspondence to jrogers@illinois.edu.

Received for review September 30, 2014 and accepted December 3, 2014.

Published online December 03, 2014
10.1021/nn505566r

© 2014 American Chemical Society

(s-SWNTs), thereby making it difficult to fabricate transistors or electronic circuits with high performance. According to tight-binding model calculations of the SWNT electronic band structure,[3,10,11] and as observed in experiment,[12,13] roughly 2/3 of all of the SWNTs are semiconducting and 1/3 are metallic. The m-SWNTs form electrical shorts that greatly diminish the on/off switching ratios of transistors that use arrays of such SWNTs as the channel material. Selective growth techniques allow arrays with enriched content of s-SWNTs[14,15] but not to an extent that excludes m-SWNTs to a degree needed for use in digital electronics, for example. One approach to eliminate m-SWNTs involves application of large bias voltages to transistors that are modulated into their nominal off state.[2,16] This process of selective electrical breakdown of the m-SWNTs, although successfully employed in circuits with as many as 178 transistors,[17] only eliminates small regions of the m-SWNTs and requires separate implementation on each device. A recently introduced alternative exploits much lower biases to drive nanoscale thermocapillary flows in organic thin films that uniformly coat the arrays. These films act as resists to enable complete large-scale elimination of m-SWNTs by reactive ion etching (RIE).[13] This scheme, referred to as thermocapillary-enabled purification (TcEP), removes all m-SWNTs and leaves s-SWNTs unmodified. A disadvantage is that the process requires multiple fabrication steps to form the transistor structures needed to induce current flow and generate the associated Joule heating only in the m-SWNTs. More recent results use microwave exposures to induce selective heating, but lithographically patterned antenna structures are required.[18] Capabilities in removing m-SWNTs in a way that improves the speed and simplicity of previously reported forms of TcEP could be of significant practical value.

In this article, we introduce a purification approach that exploits an infrared laser tuned to enable selective absorption and associated heating predominantly in the m-SWNTs. This scheme bypasses processing steps associated with other embodiments of TcEP to yield a greatly simplified, efficient, robust, and clean process. Here, photons with energies below the band gap of most s-SWNTs selectively absorb in the m-SWNTs.[19] Specifically, published data based on studies of SWNTs with average diameters of 1.4 nm suggest that absorption in m-SWNT is ~3 times higher than that in s-SWNTs at a wavelength of 2500 nm.[20] Although the absorption depends strongly on chirality and diameter, the results presented here indicate selective absorption into m-SWNTs in arrays (overall array densities are around 0.5−2 SWNTs/μm) grown on quartz, where the average diameter is ~1.2 nm[12] with a relatively narrow distribution.

A schematic illustration of the TcEP process using infrared (IR) radiation appears in Figure 1. Here, a thin (25 nm) film of α,α,α'-tris(4-hydroxyphenyl)-1-ethyl-4-isopropylbenzene deposited by thermal evaporation onto the SWNTs serves as the thermocapillary resist (Tc-resist). Details of this material and mechanisms that govern its flow induced by heating in SWNTs appear elsewhere.[13,21] A pulsed IR laser (10 ns pulses with repetition rate of 1 kHz) with an emission wavelength of 2500 nm serves as the light source. The exposure involves raster scanning the focused output (5 μm diameter spot) over a distance of 60 μm in a direction orthogonal to the orientation of the SWNTs at a rate of 0.4 μm/s. Heating the substrate to 70 °C during this process enhances the thermocapillary flow by decreasing the viscosity of the Tc-resist.[13,21] Selective IR absorption causes heating predominantly in the m-SWNTs, thereby leading to flow only in their vicinity. RIE then eliminates m-SWNTs exposed by this flow; removing the Tc-resist by washing in organic solvents completes the purification process.

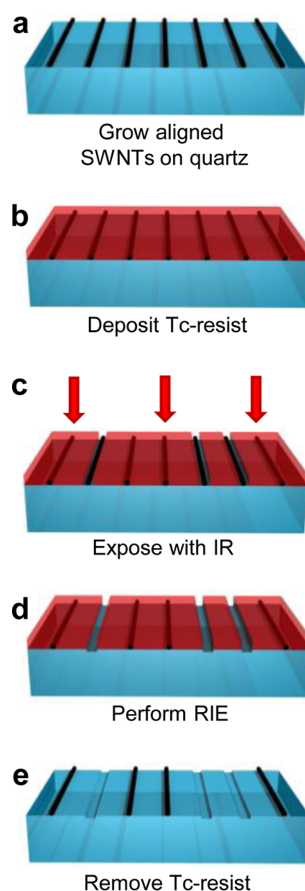

Figure 1. Schematic illustration of the laser-based TcEP process. (a) CVD growth yields aligned arrays of SWNTs formed on quartz substrates. (b) Thermal evaporation of 25 nm of α,α,α'-tris(4-hydroxyphenyl)-1-ethyl-4-isopropylbenzene (Tc-resist) establishes a uniform, conformal coating (*i.e.*, Tc-resist) on the SWNTs. (c) Focused pulsed infrared laser (λ = 2500 nm) raster scanned over the SWNTs selectively heats and induces trench formation at the m-SWNTs due to thermocapillary flows in the Tc-resist. (d) RIE selectively removes the SWNTs that are exposed by trench formation. (e) Finally, organic solvents are used to remove the Tc-resist.

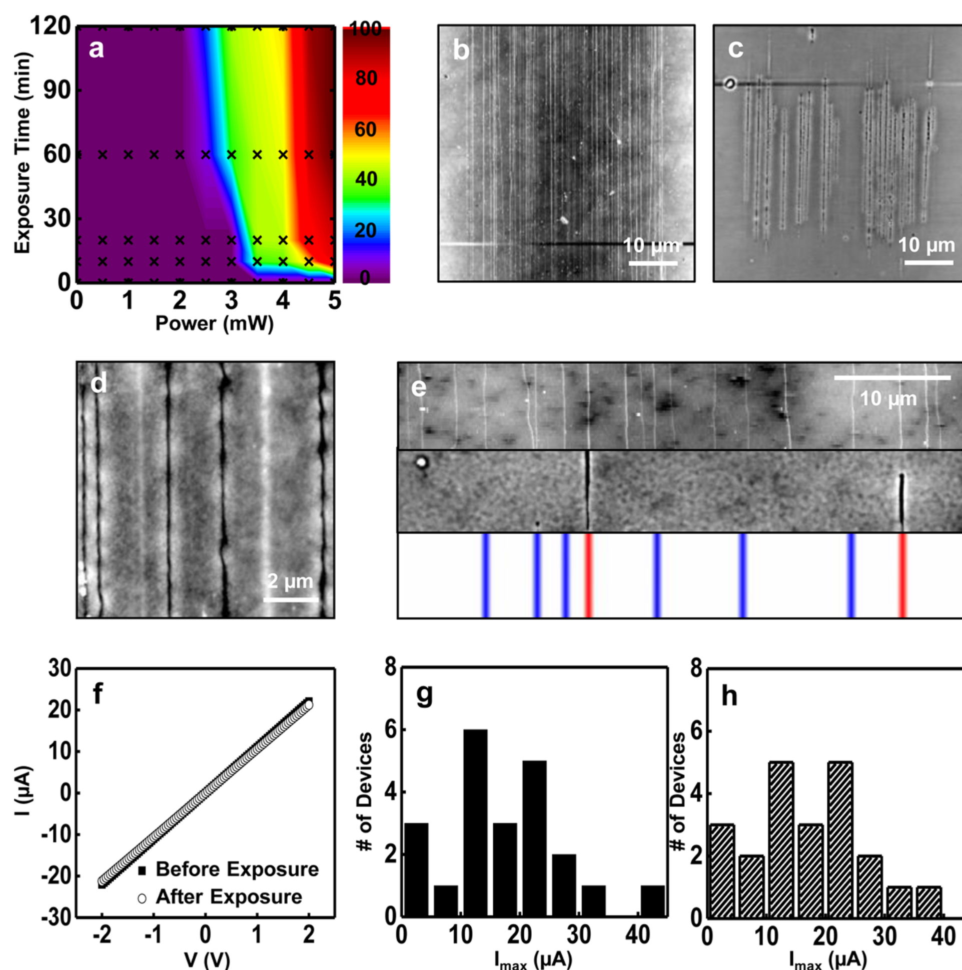

Figure 2. (a) Contour map of trench formation as a function of average laser power and exposure time. The color scale indicates the percentage of SWNTs that yield trenches. AFM images of a sample of aligned SWNTs on quartz (b) before and (c) after Tc-resist deposition and laser exposure, showing selective trench formation. (d) Magnified AFM image of a sample after trench formation, which shows selectivity in this process. (e) AFM images of SWNTs on sapphire collected before (top) and after (middle) Tc-resist deposition and trench formation. Corresponding Raman mapping of RBM modes (bottom) of m-SWNTs (red) and s-SWNTs (blue) indicate selective trench formation at positions of m-SWNTs. (f) $I-V$ characteristics for devices before and after exposure. The results indicate little to no current degradation. Histograms of I_{DS} at V_{DS} = 2 V of 22 devices before (g) and after (h) exposure.

RESULTS AND DISCUSSION

Systematic experiments conducted with various laser powers and exposure times define the optimal set of conditions. Figure 2a shows the percentage of SWNTs that yield trenches as a function of these two parameters. The violet highlighted region corresponds to little or no trench formation; green and red are regimes in which trenches form at 30−45% and ∼100% of the SWNTs, respectively. In the violet region, heating is simply insufficient to induce significant thermocapillary flow over the time scale of the experiment. In the green region, only some of the SWNTs (as shown subsequently, only the m-SWNTs) reach temperatures needed to form trenches. In the red region, both m-SWNTs and s-SWNTs form trenches. Exposures that involve durations longer than those shown here lead to wider and deeper trenches but not to formation of new trenches. The experiments described in the following involve a power of 4 mW and a rastering time of 20 min. At this chosen condition, ∼44% of SWNTs were removed, somewhat greater than the 33% of SWNTs that are expected to be m-SWNTs. A likely explanation is that the process removes some relatively small number of large diameter, defective, and/or doped s-SWNTs.

Figure 2b presents an atomic force microscope (AFM) topography image of a region of aligned SWNTs patterned by photolithography and oxygen plasma etching. Figure 2c shows the same region after Tc-resist deposition and laser exposure. Trenches (∼20 nm deep and ∼100 nm wide with variations along the SWNTs that arise from local defects and/or contamination) form at the locations of some, but not all, of the SWNTs. This observation is consistent with selective absorption. Variations in the lengths of the trench arise from the combined effects of the

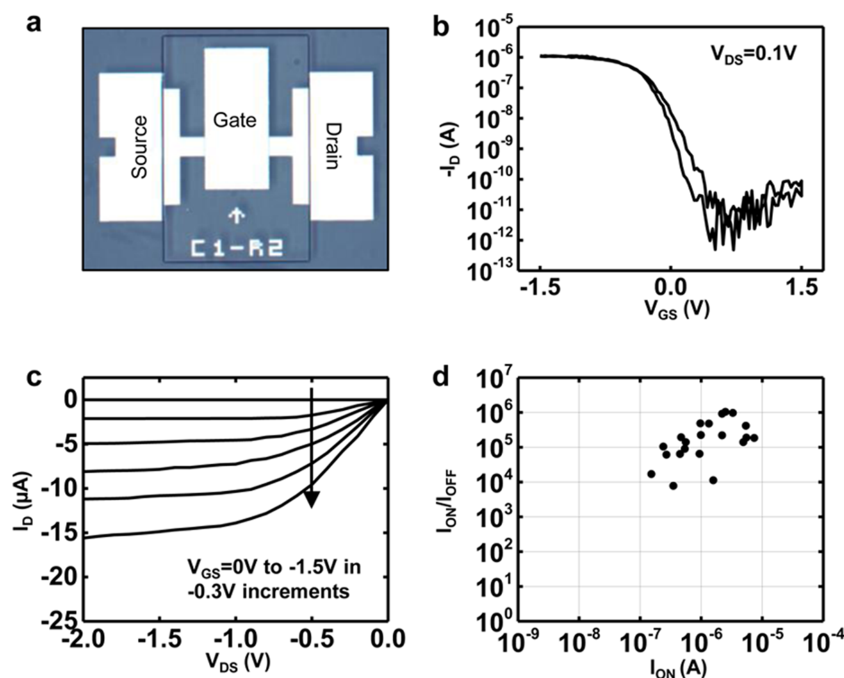

Figure 3. (a) Optical microscopy image in reflection mode of a thin-film transistor fabricated with SWNTs purified using IR-based TcEP process. (b) Transfer and (c) output characteristics of a typical SWNT TFT. (d) I_{on}/I_{off} switching ratios of 21 devices plotted *vs* I_{on} current.

Gaussian profile of the laser beam and differences in absorption coefficients among the SWNTs. Figure 2d presents a magnified view that illustrates the continuous and highly selective formation of trenches.

Raman spectroscopy establishes relationships between the formation of trenches and the diameter and electronic type of the SWNTs. The Raman measurements use SWNT arrays grown on R-plane-cut sapphire to allow direct assessment of SWNT diameter using the radial breathing mode (RBM) peak, which can be obscured by the vibrational modes in quartz. Figure 2e presents AFM images of a substrate before processing (top) and after Tc-resist deposition and laser exposure (middle), aligned with the Raman spectra (bottom). Red and blue lines correspond to RBM signals from m-SWNTs and s-SWNTs, respectively. Raman evaluation of 39 individual SWNTs, 11 from m-SWNTs and 28 from s-SWNTs, indicates that all 11 m-SWNTs yield continuous trenches, consistent with selective heating. Trenches also form at two positions that exhibit Raman signals consistent with s-SWNTs. AFM profiling indicates a height of ~4 nm at one of these locations, suggesting the presence of a bundle of two or more SWNTs and the potential for the presence of a m-SWNT. The trench at the other position might arise from absorption associated with a small band gap s-SWNT, an intraband transition, or unintentional doping. Overall, the Raman results support selective trench formation in m-SWNTs, with few exceptions.

Under nitrogen environment, laser exposure does not degrade the SWNTs, as supported by current–voltage (I–V) measurements on 22 two-terminal devices performed immediately before and after exposure, without etching any SWNTs. Results for a typical case appear in Figure 2f. Figure 2g,h shows histograms of the current (I) at a bias voltage (V) of 2 V for all devices for before and after, respectively. To within less than 5%, the current is unaltered. Transistors fabricated using these purified arrays of SWNTs provide critical information on the effectiveness of the process. An optical microscope image of a device (channel length (L) of 200 μm and width (W) of 40 μm) is shown in Figure 3a. Representative transfer and output characteristics appear in Figure 3b,c, respectively. The ratio of currents in the on and off states (I_{ON}/I_{OFF}) are >10^5, consistent with complete elimination of the m-SWNTs. Devices fabricated with pristine, unpurified SWNTs of identical SWNT density indicate on-off ratios from 2 to 4, similar to data presented in previous reports.[2,13,22] Figure 3d shows switching ratios of 21 devices similar to the one in Figure 3a. In all cases, I_{ON}/I_{OFF} is greater than ~10^4, with some values that approach 10^6, corresponding to s-SWNT purity of at least 99.8%. This lower limit is defined by the total number of SWNTs examined and most likely is significantly higher than the value reported here.

The I–V characteristics of the transistors enable extraction of the effective mobility (μ) according to

$$\mu = \frac{L}{V_D C_W W} \cdot \frac{dI_D}{dV_G}$$

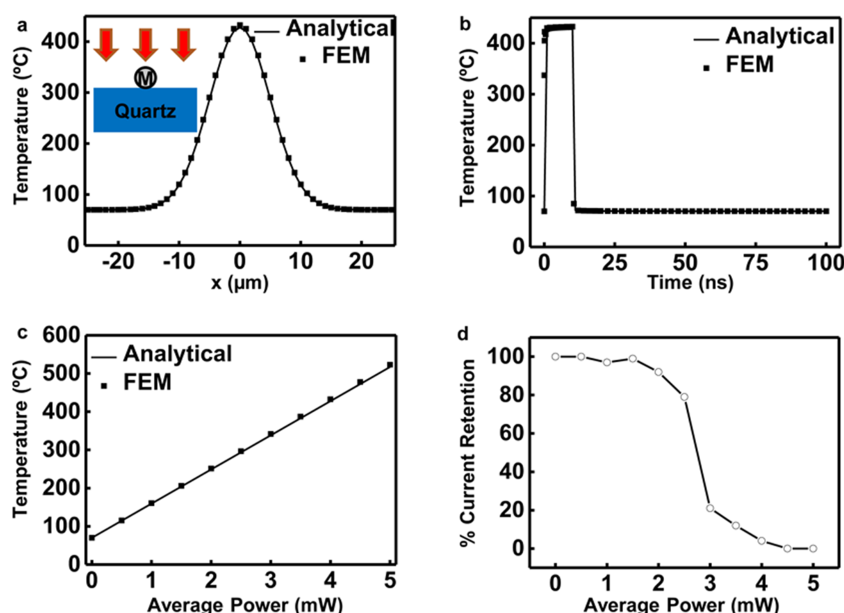

Figure 4. (a) Maximum temperature along the axis of the m-SWNT during pulsed laser exposure as calculated by analytical and finite-element thermomechanical modeling. The inset shows a schematic representation of the model, which includes bare m-SWNT on quartz. (b) Calculated maximum temperature of the m-SWNT as a function of time. (c) Calculated maximum temperature of the m-SWNTs as a function of average laser power. (d) Current retention of two terminal devices fabricated with as-grown SWNTs after exposure at varying IR laser powers. Device degradation occurs at ∼3.5 mW, corresponding to temperatures of ∼350 °C according to the models.

where the channel length $L = 150\,\mu$m and channel width $W = 60\,\mu$m. C_W is the specific capacitance per unit area of the aligned SWNT channel, which can be calculated by accounting for the s-SWNT density (D, tubes per unit width), the quantum capacitance (C_Q), and geometric capacitance (C_G) per individual s-SWNT:[23]

$$C_W = \frac{D}{[C_Q^{-1} + C_G^{-1}]}$$

$$C_G = \frac{2\pi\varepsilon_0\varepsilon_{SiO_2}}{\ln\left[\frac{D\sinh(2\pi EOT/D)}{\pi r}\right]}$$

where r is the radius of the SWNTs, ε_0 is the permittivity of free space, ε_{SiO_2} is the dielectric constant of the SiO_2, and EOT is the equivalent oxide thickness for the double-layer dielectric stacks, calculated by[24]

$$EOT_{SU\text{-}8} = r\left[\left(1+\frac{T_{SU\text{-}8}}{r}\right)^{(\varepsilon_{SiO_2}/\varepsilon_{SU\text{-}8})} - 1\right]$$

$$EOT = EOT_{SU\text{-}8} + EOT_{SU\text{-}8}\left[\left(1+\frac{T_{HfO_2}}{EOT_{SU\text{-}8}}\right)^{(\varepsilon_{SiO_2}/\varepsilon_{HfO_2})} - 1\right]$$

Here, the definition of EOT allows simplification of the electrostatics within the dielectric stack, which contains 50 nm SU-8 and 5 nm HfO_2, where $T_{(...)}$ and $\varepsilon_{(...)}$ are the nominal thickness and dielectric constant (∼25 for HfO_2[25] and ∼4 for SU-8[26,27]) for respective dielectrics. Dielectric constants for the dielectrics may vary depending on the deposition recipe for HfO_2[28] or the dilution/coating recipe for SU-8. However, even a 20% variation in dielectric constant results only in a ∼5% variation in extracted mobility. The effect of contact resistance ∼28 kΩ[3] is ignored for mobility extraction from these long-channel length devices. The devices in Figure 3d exhibit peak mobilities between ∼900 and ∼1300 cm^2 V^{-1} s^{-1}, consistent with previously reported values for devices built with pristine, unprocessed SWNTs in the long-channel length limit.[2,13,22]

Thermal modeling provides both qualitative and quantitative insights into the distributions in temperature associated with laser exposure. A simple analytical model can be constructed for the case of an individual m-SWNT on quartz, as shown in the inset of Figure 4a. Here, the m-SWNT serves as a surface heat source with power density defined by absorption of a pulsed IR laser source with a Gaussian spot, as approximated using the Beer–Lambert law with absorption coefficients from the literature. The modeled m-SWNT has length L and width $2r$, where r is the radius, as illustrated in Supporting Information Figure S2. An average laser power of P_0 corresponds to an intensity distribution $I_0(r) = P_0 t_0/2\bar{t}\pi\sigma^2\ e^{-r^2}/2\sigma^2$ for $0 < t \leq \bar{t}$ and $I_0(r) = 0$ for $\bar{t} < t \leq t_0$, where σ is the standard deviation, $\bar{t}$ is the pulse duration, and t_0 is the pulse period. The absorption coefficient of the m-SWNT can be estimated through the Beer–Lambert law $\beta = I_{absorption}/I_0 = 1 - e^{-\delta h}$, where

δ is the absorption coefficient and h is the distance the light travels through the material. For m-SWNTs, δ is approximately 10^5 cm^{-1} and h can be approximated as twice the thickness of the wall of the SWNT (~0.34 nm), which gives $\beta \approx 0.0068$. The power density of the m-SWNT ($-L/2 \leq x \leq L/2$, $-r \leq y \leq r$) is then obtained by

$$q(x,y,t) = \begin{cases} \dfrac{\beta t_0 P_0}{2\bar{t}\pi\sigma^2} e^{-x^2/2\sigma^2} & 0 < t \leq \bar{t} \\ 0 & \bar{t} < t \leq t_0 \end{cases}$$

which gives the temperature distribution of the substrate as[29]

$$T(x,y,z,t) = \begin{cases} \displaystyle\int_{\tau=0}^{t}\int_{y'=-r}^{r}\int_{x'=-L/2}^{L/2} \frac{q(x',y',\tau)}{4\rho c[\pi\alpha(t-\tau)]^{3/2}} e^{-\frac{(x-x')^2+(y-y')^2+z^2}{4\alpha(t-\tau)}} dx'dy'd\tau + T_\infty & 0 < t \leq \bar{t} \\ \displaystyle\int_{\tau=0}^{\bar{t}}\int_{y'=-r}^{r}\int_{x'=-L/2}^{L/2} \frac{q(x',y',\tau)}{4\rho c[\pi\alpha(t-\tau)]^{3/2}} e^{-\frac{(x-x')^2+(y-y')^2+z^2}{4\alpha(t-\tau)}} dx'dy'd\tau + T_\infty & \bar{t} < t \leq t_0 \end{cases}$$

where T_∞ is the ambient temperature, ρ is the substrate density, $\alpha = k/(c\rho)$ is the thermal diffusivity of the substrate with k as the thermal conductivity and c as the specific heat capacity. The temperature of the m-SWNT can be approximated as the average temperature of the heat source plus the temperature increase due to the existence of interfacial resistance

$$T(x,t) = \begin{cases} \dfrac{1}{2r}\displaystyle\int_{y=-r}^{r} T(x,y,z=0,t)dy + q/g + T_\infty & 0 < t \leq \bar{t} \\ \dfrac{1}{2r}\displaystyle\int_{y=-r}^{r} T(x,y,z=0,t)dy + T_\infty & \bar{t} < t \leq t_0 \end{cases}$$

where g is the interface thermal conductance between the m-SWNT and quartz. Here, $\bar{t} = 10$ ns, $t_0 = 1.0$ ms, $\sigma = 5$ μm, and $P_0 = 4$ mW from experiments and $k = 6$ W·m^{-1}·K^{-1}, $\rho = 2650$ kg·m^{-3}, $c = 830$ J·kg^{-1}·K^{-1}, and $g = 5 \times 10^7$ W·m^{-2}·K^{-1} from the literature.[13] The radius r of the m-SWNT is 1.0 nm. The maximum temperature occurs at $t = \bar{t}$ and can be written approximately as

$$T(x, t = \bar{t}) = \frac{\beta t_0 P_0}{2\bar{t}\pi\sigma^2}\left\{\frac{r}{\pi k}\left[3 + \mathrm{Ei}\left(\frac{r^2}{\alpha t}\right)\right] + \frac{1}{g}\right\} e^{-x^2/2\sigma^2} + T_\infty$$

where Ei is the exponential integral.

Figure 4a shows the maximum temperature evaluated along the axis of the m-SWNT. Figure 4b gives the maximum temperature along the m-SWNT (occurring at $x = 0$) *versus* time. The temperature rapidly rises to maximum at the onset of the laser pulse and cools within ~1 ns of the end of the pulse. Finite-element analysis (ABAQUS) yields similar results.

The findings of Figure 4b suggest that the SWNTs completely cool to the ambient temperature between pulses, without appreciable cumulative heating. Figure 4c shows the maximum temperature as a function of laser power. The model suggests that the temperature can reach ~400 °C, which is sufficient to degrade SWNTs in air.[30] Measurements on two-terminal devices exposed at various laser powers in air (Figure 4d) confirm that current degradation begins at ~3 mW, corresponding to a maximum temperature of ~350 °C, consistent with the model. By rastering the laser for 20 min over a distance of 60 μm, this experiment directly simulates the exposure conditions of the TcEP process.

Finite-element results for the complete system (see Supporting Information), including the Tc-resist, appear in Figure 5a. The maximum temperature, 370 °C, is only slightly lower than that for the case of the bare m-SWNT described above. The temporal evolution of the temperature of the m-SWNT is also similar. The Tc-resist, by contrast, exhibits a time delayed thermal response due to thermal diffusion. Here, heating and cooling occurs within ~10 ns, still insignificant compared to the time between laser pulses (1 ms). The temperature distribution at the top surface of the Tc-resist is in Figure 5b. The spatial range of the temperature increase and the temperature gradient is ~100 nm (Figure S3), which is comparable to the trench widths observed in experiments. The maximum temperature is ~17 °C and occurs directly above the SWNT. This value is in the same range as, but somewhat higher than, that estimated for the case of TcEP based on heating induced by electrical current (~5 °C). Although trench formation by laser exposure might be possible at reduced temperatures, the duration of the process would be unacceptable due to the decreased rates of flow. For constant heating by electrical current, trench formation occurs in ~5 min at low temperatures. Because the laser pulse duration is only 0.1% of the period, estimated exposure times to form trenches would be ~3.5 days for similar induced temperatures.

Another consequence of the high temperatures is that they can induce chemical modification in the Tc-resist in the immediate vicinity of the m-SWNTs. Heating a test structure that consists of a film of Tc-resist (capped with a thin layer of Au to prevent sublimation) to ~200 °C reveals the effects. After removing the Au, thorough washing with organic solvent fails to fully remove the Tc-resist (Figure S1). This finding suggests that similar chemical changes are likely the cause of the residue often observed near the m-SWNTs after laser

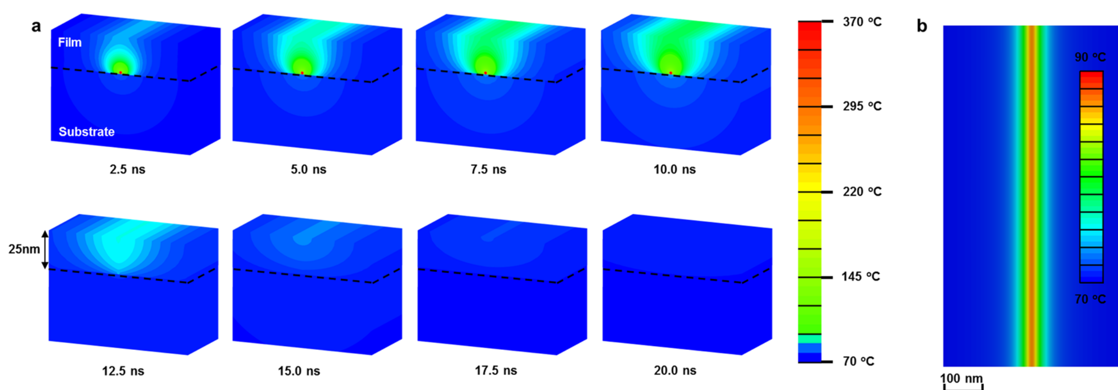

Figure 5. (a) Finite-element modeling of temperature distribution of a sample consisting of m-SWNT coated by 25 nm Tc-resist on quartz during IR pulsed laser exposure. The average laser power is 4 mW with a pulse duration of 10 ns and period of 1 ms. The cross sectional face is located at the center of of the laser spot ($x = 0$). (b) Maximum temperature distribution across the top of the Tc-resist film.

exposure. Use of a continuous wave laser at lower power could potentially avoid such effects by enabling operation at reduced temperatures.

Furthermore, the duty cycle of the laser determines the throughput of the TcEP process. The use of a continuous wave laser would increase throughput by 1000 times compared to that reported here. Additionally, optimization of Tc-resist chemistry and thickness to decrease the temperature threshold for thermocapillary flow and increase the flow rate offers further potential to decrease the time required for the process.

We note that the modeling results presented here simply provide guidance on underlying aspects of the process. The predicted temperatures depend critically on various parameters extracted from the experiments and from the literature. For example, the maximum temperatures increase exponentially with increasing absorption coefficient. Few reliable measurements of single-SWNT absorption coefficients exist.[20] In addition, reported values for the thermal interfacial conductance for SWNTs span a wide range, from 3×10^7 to 1×10^8 W·m^{-2}·K^{-1}. Corresponding temperatures of m-SWNTs predicted by finite-element modeling vary from 250 to 450 °C within this range. The maximum temperature at the top of the film, which is critical for thermocapillary flow, is, by contrast, largely insensitive to thermal interfacial conductance, with a variation of less than 5 °C for this same range. Overall, the good correspondence between calculations and experimental observations supports the validity of the models and the materials parameters used here.

CONCLUSIONS

In summary, this paper demonstrates a robust and clean process for removing m-SWNTs from as-grown aligned arrays of SWNTs. The use of readily available lasers and materials makes this process fully compatible with processing approaches that are already in widespread use in the semiconductor industry. The trenches are approximately 100 nm wide; for densities higher than 10 SWNT/μm, such widths are sufficient to lead to significant unintentional removal of s-SWNTs. Decreasing the widths by use of optimized chemistries and thicknesses of the Tc-resist or performing purification on arrays with enriched content of s-SWNTs[31] can reduce effects, thereby allowing efficient application to SWNTs at densities significantly higher than 10 SWNT/μm.[32−34] Opportunities for future work include exploration of other wavelengths for enhanced selectivity, alternative laser sources for scaling and throughput of the purification process, and most importantly, optimized power and pulse durations to facilitate trench formation.

METHODS

Synthesis of Aligned Arrays of SWNTs on Quartz. ST-cut single-crystal quartz substrates (Hoffman Materials, Inc.) were thermally annealed in air at 900 °C for 12 h. Narrow stripes of Fe catalysts (2 Å) were formed on annealed quartz substrates by electron beam evaporation (AJA ATC Orion 8E) and photolithography (AZ 5214E and Suss Microtech MJB 3). Heating at 900 °C for 1 h in the reaction chamber induced formation of Fe nanoparticles. After the substrate was cooled to room temperature, heating to 925 °C under hydrogen gas flow with 400 sccm for 10 min fully reduced the catalyst. Chemical vapor deposition growth was performed by flowing Ar (30 sccm) and H_2 (30 sccm) through an ethanol bubbler at 925 °C for 30 min.

Synthesis of Aligned Arrays of SWNTs on Sapphire. R-plane-cut single-crystal sapphire substrates (Marketech International Inc.) were thermally annealed in air at 900 °C for 24 h. The remaining procedures for growth were identical to those used with quartz.

Raman Spectroscopy. Raman spectroscopy was conducted using a confocal micro-Raman system (Horiba LabRAM HR) at 532, 633, and 785 nm wavelengths. Lasers with 1 μm spot sizes were rastered in 0.5 μm steps to map the radial breathing mode of SWNTs across the substrate.

Thermocapillary Resist Deposition. Deposition of 25 nm of α,α,α′-tris(4-hydroxyphenyl)-1-ethyl-4-isopropylbenzene was conducted *via* thermal evaporation at a rate of 0.5 Å/s.

Laser Exposure. Transparent resistive heaters were fabricated using ITO glass slides (Sigma-Aldrich, USA) with patterned

electrodes along opposite edges. These heaters were contacted to the back sides of the SWNT substrates. Voltage was applied to increase the temperature of the SWNT substrate to 70 °C, as measured by type K thermocouples on the surface of the quartz. Nitrogen gas was gently flowed (<5 psi) over the surface of the substrate to prevent oxidation and degradation of SWNTs during laser exposure and thermocapillary flow. The substrate and heater were magnetically attached to a mechanical stage. Exposures were performed using a pulsed laser with wavelength of 2500 nm, pulse duration of 10 ns, repetition rate of 1 kHz, and spot size of 5 μm (Anasys nanoIR).

Selective Etching of m-SWNTs. Dry etching of SWNTs after laser exposure and trench formation was conducted using RIE (PlasmaTherm SLR-730): 5 sccm CF4, 1 sccm O_2, 10 mTorr, 80 W, 17 s.

Device Fabrication. SWNTs were patterned into regions with dimensions of 40 μm by 350 μm *via* photolithography (AZ 5214E and Suss Microtech MJB 4) and O_2 plasma etching (MARCH CS-1701 RIE). The 2 nm Ti and 50 nm Pd bilayer contacts were deposited by electron beam evaporation (AJA ATC Orion 8E) and patterned into electrodes with widths of 60 μm and spacings of 150 μm apart by photolithography (AZ 5214E and Suss Microtech MJB 4) and lift-off processing. The gate dielectric was formed by spin coating a 50 nm thick film of a photodefinable epoxy (SU-8, 1:7 MicroChem SU-8 2002 diluted in hexane) and baking at 250 °C for 1 h in a glovebox. Then, 20 nm HfO_2 was subsequently deposited at 120 °C *via* atomic layer deposition (Cambridge Nanotech Savannah). The bilayer dielectric uses a scheme previously optimized to reduce hysteresis in SWNT field-effect transistors.[35] The 2 nm Ti and 50 nm Au bilayer gate contacts were deposited by electron beam evaporation (AJA ATC Orion 8E) and patterned by photolithography (AZ 5214E and Suss Microtech MJB 4) and lift-off. Removal of the dielectric material over the source and drain contacts was performed by photolithography followed by RIE (PlasmaTherm SLR-730).

Experimental Study of Residual Films after Trench Formation. The elevated temperatures at the SWNT–Tc-resist interface can lead to chemical or physical modification or degradation to the Tc-resist material, resulting in a residual film after trench formation. To confirm this hypothesis, we utilized samples shown in Figure S1a. Here, a 25 nm thick overcoat of gold deposited by electron beam evaporation prevents sublimation of the underlying Tc-resist during heating induced by a hot plate. Experiments were conducted in a glovebox under nitrogen atmosphere, with heating for 10 min at various temperatures. After heating, the samples were placed into an acetone bath for 1 h followed by aggressive washing with acetone, isopropyl alcohol (IPA), deionized water, and then IPA. In all samples, the gold film delaminated easily due to poor adhesion with the Tc-resist directly underneath. AFM examination of the resulting substrate revealed any remaining residue. The thickness of the residue is plotted *versus* baking temperature in Figure S1b. For temperatures greater than 200 °C, the film becomes impossible to remove using the aggressive solvent wash. The temperature of the m-SWNTs during IR exposure, as predicted by analytical and FEA modeling, exceeds these values, indicating that this heating is likely the cause of the residual film that is often observed at the bottoms of the trenches after IR-based TcEP processing.

Finite-Element Modeling. A three-dimensional finite-element model is established to study the temperature distribution in the system and validate the analytical model. Eight-node, hexahedral brick elements in the finite-element software ABAQUS are used to discretize the geometry. A volume heat source with Gaussian distribution along the axis of m-SWNT is applied on the m-SWNT. A constant temperature is applied at the bottom of the quartz substrate, and all the other boundaries are thermal convection boundary with the coefficient of heat convection 25 $W \cdot m^{-2} \cdot K^{-1}$. The Tc-resist has thermal conductivity, density, and specific heat capacity of 0.2 $W \cdot m^{-1} \cdot K^{-1}$, 1160 $kg \cdot m^{-3}$, and 1500 $J \cdot kg^{-1} \cdot K^{-1}$[13] and the m-SWNT has 4000 $W \cdot m^{-1} \cdot K^{-1}$, 1300 $kg \cdot m^{-3}$, and 400 $J \cdot kg^{-1} \cdot K^{-1}$.[13,36] The finite-element simulations agree well with analytical modeling as shown in Figure 4 for the system of a m-SWNT on a bare quartz substrate.

Conflict of Interest: The authors declare no competing financial interest.

Acknowledgment. We thank D. Wibawa and P. Sanghani for catalyst patterning and deposition and aligned SWNT CVD growth. This material is based upon work supported by the SONIC program (laser purification) and by Northrop Grumman (device fabrication and test). The work used facilities in the Frederick Seitz Materials Research Lab and the Center for Microanalysis of Materials at the University of Illinois.

Supporting Information Available: Additional information on the finite-element modeling and on the experiments about Tc-resist residues. This material is available free of charge *via* the Internet at http://pubs.acs.org.

REFERENCES AND NOTES

1. Avouris, P.; Chen, Z. H.; Perebeinos, V. Carbon-Based Electronics. *Nat. Nanotechnol.* **2007**, *2*, 605–615.
2. Kang, S. J.; Kocabas, C.; Ozel, T.; Shim, M.; Pimparkar, N.; Alam, M. A.; Rotkin, S. V.; Rogers, J. A. High-Performance Electronics Using Dense, Perfectly Aligned Arrays of Single-Walled Carbon Nanotubes. *Nat. Nanotechnol.* **2007**, *2*, 230–236.
3. Zhou, X. J.; Park, J. Y.; Huang, S. M.; Liu, J.; McEuen, P. L. Band Structure, Phonon Scattering, and the Performance Limit of Single-Walled Carbon Nanotube Transistors. *Phys. Rev. Lett.* **2005**, *95*, 146805.
4. Tans, S. J.; Verschueren, A. R. M.; Dekker, C. Room-Temperature Transistor Based on a Single Carbon Nanotube. *Nature* **1998**, *393*, 49–52.
5. Kocabas, C.; Hur, S. H.; Gaur, A.; Meitl, M. A.; Shim, M.; Rogers, J. A. Guided Growth of Large-Scale, Horizontally Aligned Arrays of Single-Walled Carbon Nanotubes and Their Use in Thin-Film Transistors. *Small* **2005**, *1*, 1110–1116.
6. Xiao, J. L.; Dunham, S.; Liu, P.; Zhang, Y. W.; Kocabas, C.; Moh, L.; Huang, Y. G.; Hwang, K. C.; Lu, C.; Huang, W.; Rogers, J. A. Alignment Controlled Growth of Single-Walled Carbon Nanotubes on Quartz Substrates. *Nano Lett.* **2009**, *9*, 4311–4319.
7. Alam, M. A.; Pimparkar, N.; Kumar, S.; Murthy, J. Theory of Nanocomposite Network Transistors for Macroelectronics Applications. *MRS Bull.* **2006**, *31*, 466–470.
8. Hu, L.; Hecht, D. S.; Gruner, G. Percolation in Transparent and Conducting Carbon Nanotube Networks. *Nano Lett.* **2004**, *4*, 2513–2517.
9. Nirmalraj, P. N.; Lyons, P. E.; De, S.; Coleman, J. N.; Boland, J. J. Electrical Connectivity in Single-Walled Carbon Nanotube Networks. *Nano Lett.* **2009**, *9*, 3890–3895.
10. Hamada, N.; Sawada, S.; Oshiyama, A. New One-Dimensional Conductors—Graphitic Microtubules. *Phys. Rev. Lett.* **1992**, *68*, 1579–1581.
11. Saito, R.; Fujita, M.; Dresselhaus, G.; Dresselhaus, M. S. Electronic-Structure of Chiral Graphene Tubules. *Appl. Phys. Lett.* **1992**, *60*, 2204–2206.
12. Islam, A. E.; Du, F.; Ho, X. N.; Jin, S. H.; Dunham, S.; Rogers, J. A. Effect of Variations in Diameter and Density on the Statistics of Aligned Array Carbon-Nanotube Field Effect Transistors. *J. Appl. Phys.* **2012**, *111*, 054511.
13. Jin, S. H.; Dunham, S. N.; Song, J. Z.; Xie, X.; Kim, J. H.; Lu, C. F.; Islam, A.; Du, F.; Kim, J.; Felts, J.; Li, Y. H.; Xiong, F.; Wahab, M. A.; Menon, M.; Cho, E.; Grosse, K. L.; Lee, D. J.; Chung, H. U.; Pop, E.; Alam, M. A.; King, W. P.; Huang, Y. G.; Rogers, J. A. Using Nanoscale Thermocapillary Flows To Create Arrays of Purely Semiconducting Single-Walled Carbon Nanotubes. *Nat. Nanotechnol.* **2013**, *8*, 347–355.
14. Ding, L.; Tselev, A.; Wang, J.; Yuan, D.; Chu, H.; McNicholas, T. P.; Li, Y.; Liu, J. Selective Growth of Well-Aligned Semiconducting Single-Walled Carbon Nanotubes. *Nano Lett.* **2009**, *9*, 800–805.
15. Liu, J.; Wang, C.; Tu, X.; Liu, B.; Chen, L.; Zheng, M.; Zhou, C. Chirality-Controlled Synthesis of Single-Wall Carbon

Nanotubes Using Vapour-Phase Epitaxy. *Nat. Commun.* **2012**, *3*, 1199.
16. Collins, P. C.; Arnold, M. S.; Avouris, P. Engineering Carbon Nanotubes and Nanotube Circuits Using Electrical Breakdown. *Science* **2001**, *292*, 706–709.
17. Shulaker, M. M.; Hills, G.; Patil, N.; Wei, H.; Chen, H. Y.; PhilipWong, H. S.; Mitra, S. Carbon Nanotube Computer. *Nature* **2013**, *501*, 526–530.
18. Xie, X.; Jin, S. H.; Wahab, M. A.; Islam, A. E.; Zhang, C. X.; Du, F.; Seabron, E.; Lu, T. J.; Dunham, S.; Chen, H. I.; Tu, I. C.; Guo, Z. L.; Chung, H. U.; Li, Y. H.; Liu, Y. H.; Lee, J. H.; Song, J. Z.; Huang, Y. G.; Alam, M. A.; Wilson, W. L.; Rogers, J. A. Microwave Purification of Large-Area, Horizontally Aligned Arrays of Single-Walled Carbon Nanotubes. *Nat. Commun.* **2014**, *5*, 5332.
19. Kataura, H.; Kumazawa, Y.; Maniwa, Y.; Umezu, I.; Suzuki, S.; Ohtsuka, Y.; Achiba, Y. Optical Properties of Single-Wall Carbon Nanotubes. *Synth. Met.* **1999**, *103*, 2555–2558.
20. Ichida, M.; Saito, S.; Nakano, T.; Feng, Y.; Miyata, Y.; Yanagi, K.; Kataura, H.; Ando, H. Absorption Spectra of High Purity Metallic and Semiconducting Single-Walled Carbon Nanotube Thin Films in a Wide Energy Region. *Solid State Commun.* **2011**, *151*, 1696–1699.
21. Jin, S. H.; Song, J. Z.; Chung, H. U.; Zhang, C. X.; Dunham, S. N.; Xie, X.; Du, F.; Kim, T. I.; Lee, J. H.; Huang, Y. G.; Rogers, J. A. Fundamental Effects in Nanoscale Thermocapillary Flow. *J. Appl. Phys.* **2014**, *115*, 054315.
22. Ho, X. N.; Ye, L. N.; Rotkin, S. V.; Cao, Q.; Unarunotai, S.; Salamat, S.; Alam, M. A.; Rogers, J. A. Scaling Properties in Transistors That Use Aligned Arrays of Single-Walled Carbon Nanotubes. *Nano Lett.* **2010**, *10*, 499–503.
23. Cao, Q.; Xia, M. G.; Kocabas, C.; Shim, M.; Rogers, J. A.; Rotkin, S. V. Gate Capacitance Coupling of Singled-Walled Carbon Nanotube Thin-Film Transistors. *Appl. Phys. Lett.* **2007**, *90*, 023516.
24. Tienda-Luna, I. M.; Ruiz, F. J. G.; Donetti, L.; Godoy, A.; Gamiz, F. Modeling the Equivalent Oxide Thickness of Surrounding Gate SOI Devices with High-Kappa Insulators. *Solid-State Electron.* **2008**, *52*, 1854–1860.
25. Wilk, G. D.; Wallace, R. M.; Anthony, J. M. High-Kappa Gate Dielectrics: Current Status and Materials Properties Considerations. *J. Appl. Phys.* **2001**, *89*, 5243–5275.
26. Thorpe, J. R.; Steenson, D. P.; Miles, R. E. High Frequency Transmission Line Using Micromachined Polymer Dielectric. *Electron. Lett.* **1998**, *34*, 1237–1238.
27. Processing Guidelines for SU-8 2000.5, **2014**.
28. Hsu, C. T.; Su, Y. K.; Yokoyama, M. High Dielectric-Constant of Rf-Sputtered HfO_2 Thin-Films. *Jpn. J. Appl. Phys.* **1992**, *31*, 2501–2504.
29. Carslaw, H. S.; Jaeger, J. C. *Conduction of Heat in Solids*, 2nd ed.; Clarendon Press: Oxford, 1959; p 510.
30. Duong, H. M.; Einarsson, E.; Okawa, J.; Xiang, R.; Maruyama, S. Thermal Degradation of Single-Walled Carbon Nanotubes. *Jpn. J. Appl. Phys.* **2008**, *47*, 1994–1999.
31. Li, J.; Liu, K.; Liang, S.; Zhou, W.; Pierce, M.; Wang, F.; Peng, L.; Liu, J. Growth of High-Density-Aligned and Semiconducting-Enriched Single-Walled Carbon Nanotubes Decoupling the Conflict between Density and Selectivity. *ACS Nano* **2014**, *8*, 554–562.
32. Shekhar, S.; Erementchouk, M.; Leuenberger, M. N.; Khondaker, S. I. Correlated Electrical Breakdown in Arrays of High Density Aligned Carbon Nanotubes. *Appl. Phys. Lett.* **2011**, *98*, 243121.
33. Shekhar, S.; Stokes, P.; Khondaker, S. I. Ultrahigh Density Alignment of Carbon Nanotube Arrays by Dielectrophoresis. *ACS Nano* **2011**, *5*, 1739–1746.
34. Cao, Q.; Han, S. J.; Tulevski, G. S. Fringing-Field Dielectrophoretic Assembly of Ultrahigh-Density Semiconducting Nanotube Arrays with a Self-Limited Pitch. *Nat. Commun.* **2014**, *5*, 5071.
35. Jin, S. H.; Islam, A. E.; Kim, T.-i.; Kim, J.-h.; Alam, M. A.; Rogers, J. A. Sources of Hysteresis in Carbon Nanotube Field-Effect Transistors and Their Elimination *via* Methylsiloxane Encapsulants and Optimized Growth Procedures. *Adv. Funct. Mater.* **2012**, *22*, 2276–2284.
36. Pipes, R. B.; Frankland, S. J. V.; Hubert, P.; Saether, E. Self-Consistent Properties of Carbon Nanotubes and Hexagonal Arrays as Composite Reinforcements. *Compos. Sci. Technol.* **2003**, *63*, 1349–1358.